Nanoscale Res Lett (2010) 5:383–388
DOI 10.1007/s11671-009-9493-5

NANO EXPRESS

Side-by-Side $In(OH)_3$ and In_2O_3 Nanotubes: Synthesis and Optical Properties

Xiaojun Tao · Lei Sun · Zhiwei Li · Yanbao Zhao

Received: 13 October 2009 / Accepted: 11 November 2009 / Published online: 27 November 2009

Abstract A simple and mild wet-chemical approach was developed for the synthesis of one-dimensional (1D) $In(OH)_3$ nanostructures. By calcining the 1D $In(OH)_3$ nanocrystals in air at 250 °C, 1D In_2O_3 nanocrystals with the same morphology were obtained. TEM results show that both 1D $In(OH)_3$ and 1D In_2O_3 are composed of uniform nanotube bundles. SAED and XRD patterns indicate that 1D $In(OH)_3$ and 1D In_2O_3 nanostructures are single crystalline and possess the same bcc crystalline structure as the bulk $In(OH)_3$ and In_2O_3, respectively. TGA/DTA analyses of the precursor $In(OH)_3$ and the final product In_2O_3 confirm the existence of CTAB molecules, and its content is about 6%. The optical absorption band edge of 1D In_2O_3 exhibits an evident blueshift with respect to that of the commercial In_2O_3 powders, which is caused by the increasing energy gap resulted from decreasing the grain size. A relatively strong and broad purple-blue emission band centered at 440 nm was observed in the room temperature PL spectrum of 1D In_2O_3 nanotube bundles, which was mainly attributed to the existence of the oxygen vacancies.

Keywords Side-by-side · $In(OH)_3$ · In_2O_3 · Nanotubes · Wet-chemical approach

Introduction

One-dimensional nanostructures (1D: nanostructures with nanometer-sized diameters but much longer lengths), such as nanorods/nanowires, nanotubes, and nanobelts have been extensively prepared and investigated, owing to their unusual chemical and physical properties that differ from those of the bulk materials and potential utilization in nanoelectronic and optoelectronic devices [1–11]. In recent years, much attention has been paid to the fabrication and self-assembly of 1D wide-bandgap semiconducting oxides because of their interesting optical and electronic feature [10–13], including fabrication of semiconductor materials with hollow and core–shell structures [14–16]. Especially, indium hydroxide $In(OH)_3$ (with a wide-bandgap about 5.15 eV) [17] and indium oxide In_2O_3 (with a direct bandgap around 3.6 eV and an indirect bandgap around 2.5 eV) [18–24], as two important wide-bandgap semiconductor, are of great importance for fundamental research and many device applications such as solar cell [25], organic light-emitting diodes [26–28], architectural glasses [27], gas sensors [29], and flat-panel display [25, 30]. Accordingly, various type of synthetical strategies have been established for synthesizing one-dimensional $In(OH)_3$ and In_2O_3 nanostructures, such as sonohydrolysis, chemical vapor deposition, hydrothermal method, and these methods often require special equipment and rigorous experimental condition [17, 31–34]. Moreover, among the reported literatures, the research on the solution phase fabrication of 1D $In(OH)_3$ and 1D In_2O_3 nanotubes is rather limited. Therefore, the solution phase synthesis of 1D $In(OH)_3$ and 1D In_2O_3 nanotubes remains a challenging task.

In this study, we report a facile wet-chemical synthesis of well-defined 1D $In(OH)_3$ nanotubes from the hydrolysis of the $In(NO_3)_3{\cdot}4.5H_2O$ precursor in the presence of surfactant cetyltrimethylammonium bromide (CTAB). Meanwhile, we found that the as-synthesized 1D precursor $In(OH)_3$ nanostructures easily turned into In_2O_3

X. Tao (✉) · L. Sun · Z. Li · Y. Zhao
Key Laboratory for Special Functional Materials, Henan University, 475004 Kaifeng, China
e-mail: xjtao819@163.com

nanostructures with the same shape. The optical properties of 1D In_2O_3 nanotube bundles were also studied.

Experimental Section

Preparation of the Precursor $In(OH)_3$ Nanostructures

First, 0.38 g (0.001 mol) of $In(NO_3)_3{\cdot}4.5H_2O$ was dissolved in 80 mL of distilled water, and 0.36 g (0.001 mol) cetyltrimethylammonium bromide (CTAB) was dissolved in 20 mL of ethanol (95%). Secondly, two solutions were introduced into a round-bottom three-neck flask equipped with the condensator and magnetic stirring. Then, the mixture was heated to reflux. Gradually, the solution turned from colorless and transparent to white turbid. After the reaction was lasted for 12 h, the white turbid solution was centrifugated at 10,000 rpm and washed with anhydrous ethanol several times. Finally, the white powders obtained were dried in an air atmosphere at 60 °C for 12 h.

Transformation of $In(OH)_3$ Nanostructures into In_2O_3 Nanostructures

The appropriate amount of the precursor $In(OH)_3$ nanostructures were coated on a clean glass flake as thin as possible. This glass flake was transferred into an oven (air atmosphere), in which temperature was kept at 250 °C for 8 h. Under the current condition, the dehydration of the precursor $In(OH)_3$ nanostructures was complete and the light yellow In_2O_3 nanostructures were obtained.

Characterization Techniques

The X-ray powder diffraction pattern was recorded with an X-ray diffractometer (Philips) using Cu Kα (40 kV $\times$ 40 mA) radiation ($\lambda = 0.154056$ nm). Low-magnification and high-magnification TEM images were taken on JEM-100CXII (using an accelerating voltage of 100 Kv) and JEM-2010 (using an accelerating voltage of 200 Kv) transmission electron microscope, respectively. SAED images were carried out on JEM-100CXII. A UV–visible spectrophotometer, HEλIOSa was used to carry out the optical measurement of the sample dispersed in $CHCl_3$. The room temperature PL spectrum was performed on a SPEX F212 fluorescence spectrophotometer with a Xe lamp upon excitation at 300 nm.

Results and Discussion

Figure 1a presents the XRD pattern of the $In(OH)_3$ precursor. All of the detectable reflection peaks match well with those of a body-centered cubic phase [space group: $Im\underline{3}$ (204)] $In(OH)_3$ (JCPDS card no. 85-1338), and the peak intensities are consistent with those of the standard materials except that the relative intensity of (220)/(420) peak is a little more intense. Figure 1b shows the XRD pattern of the In_2O_3 nanostructures obtained by calcination of the as-made $In(OH)_3$. All of the diffraction peaks can be readily indexed to body-centered cubic phase [space group: $Ia\underline{3}$ (206)] of In_2O_3 with cell parameter of $a = 10.116$ Å, which is in very agreement with the literature values of $a = 10.11$ Å (JCPDS card no. 71-2195). Here, the relative intensity of (400)/(622) peak is a little more intense.

Figure 2a is the typical TEM image of $In(OH)_3$ precursor. The morphology of the as-prepared precursor $In(OH)_3$ is short and relatively uniform belts with an average diameter of 55 nm and a mean length of 180 nm. Interestingly, a typically local magnified image (Fig. 2b) and TEM image with larger magnification (Fig. 2c) clearly reveal that the as-synthesized 1D $In(OH)_3$ nanostructures virtually are side-by-side nanotube bundles consisting of $In(OH)_3$ nanotubes with the smaller size in diameter rather than genuine belts. The representative electron diffraction pattern (Fig. 2d) corresponding to a bundle of nanotubes shows diffraction rings consisting of strong spots, indicating that 1D $In(OH)_3$ nanostructures are essentially single crystalline.

The TEM morphology of the In_2O_3 sample was shown in Fig. 3a. Obviously, after the precursor $In(OH)_3$ nanotube bundles were calcined in the air, the morphology of the nanotube bundles was successfully inherited in the transformation from $In(OH)_3$ to In_2O_3. However, the size of the In_2O_3 products is slightly smaller than that of the $In(OH)_3$ precursor owing to the dehydration of the $In(OH)_3$ precursor in calcination. A typically local magnified image of the area marked by the white arrow (Fig. 3b) and TEM

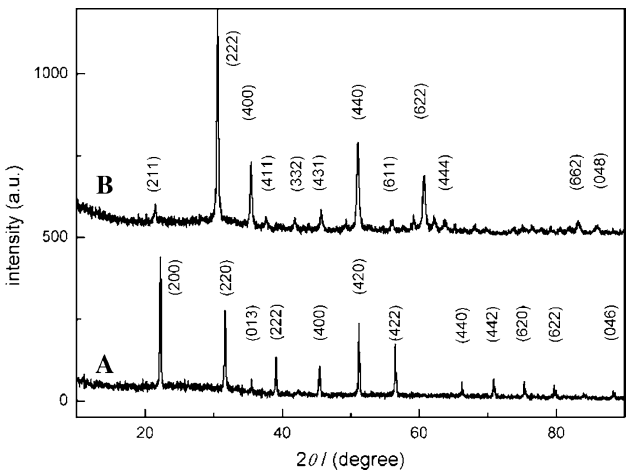

Fig. 1 XRD patterns of the precursor $In(OH)_3$ (**a**) and the final product In_2O_3 (**b**)

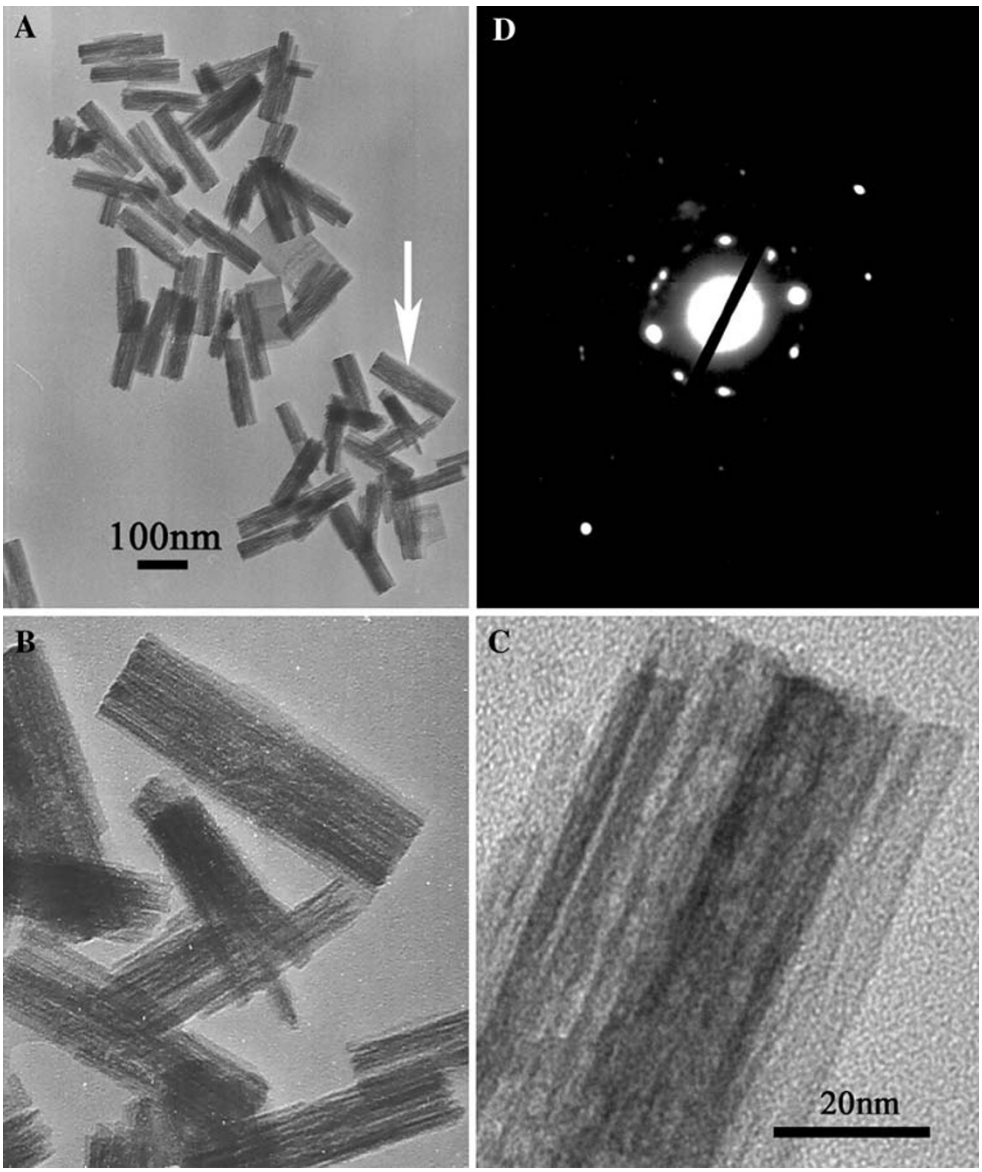

Fig. 2 **a** The typical TEM picture of the precursor $In(OH)_3$. **b**, **c** Correspond to the enlarged image of the area marked by the *white arrow* in **a** and TEM image with larger magnification, respectively. **d** The selected area electronic diffraction pattern of $In(OH)_3$

image with larger magnification (Fig. 3c) forcefully supported the earlier explanation. To investigate the crystallinity of the as-prepared In_2O_3 nanotube bundles, the selected area electron diffraction (Fig. 3d) was recorded on a bundle of In_2O_3 nanotubes. The strong and symmetrical diffraction spots can be easily indexed to the bcc structure of In_2O_3, which reveal that 1D In_2O_3 nanostructures are essentially single crystalline.

Figure 4 gives TGA/DTA curves of the precursor $In(OH)_3$. The TGA curve can be mainly divided into three weight-loss steps. The first step from room temperature to 150 °C is due to the desorption of absorbed alcohol and water molecules on the sample powder. The second step between 150 and 300 °C shows a ~16% weight loss, which is in good agreement with theoretical value and the literature report [35]. Corresponding to DTA curve, there exists an endothermic peak at 270 °C, which is related to the decomposition of the hydroxide to the indium oxide. The last weight-loss step from 300 to 800 °C (about 6%) should be attributed to the decomposition of CTAB molecules which are chemically bonded to $In(OH)_3$. In order to further determine the content of the CTAB molecules, the final product In_2O_3 was also studied via TGA/DTA, as shown in Fig. 5. The TGA curve gives a weight loss of about 6% between 250 and 800 °C, and the DTA curve shows an exothermic peak at 420 °C, which could be attributed to burning off the organic component. This result is consistent with that of the precursor $In(OH)_3$. Through

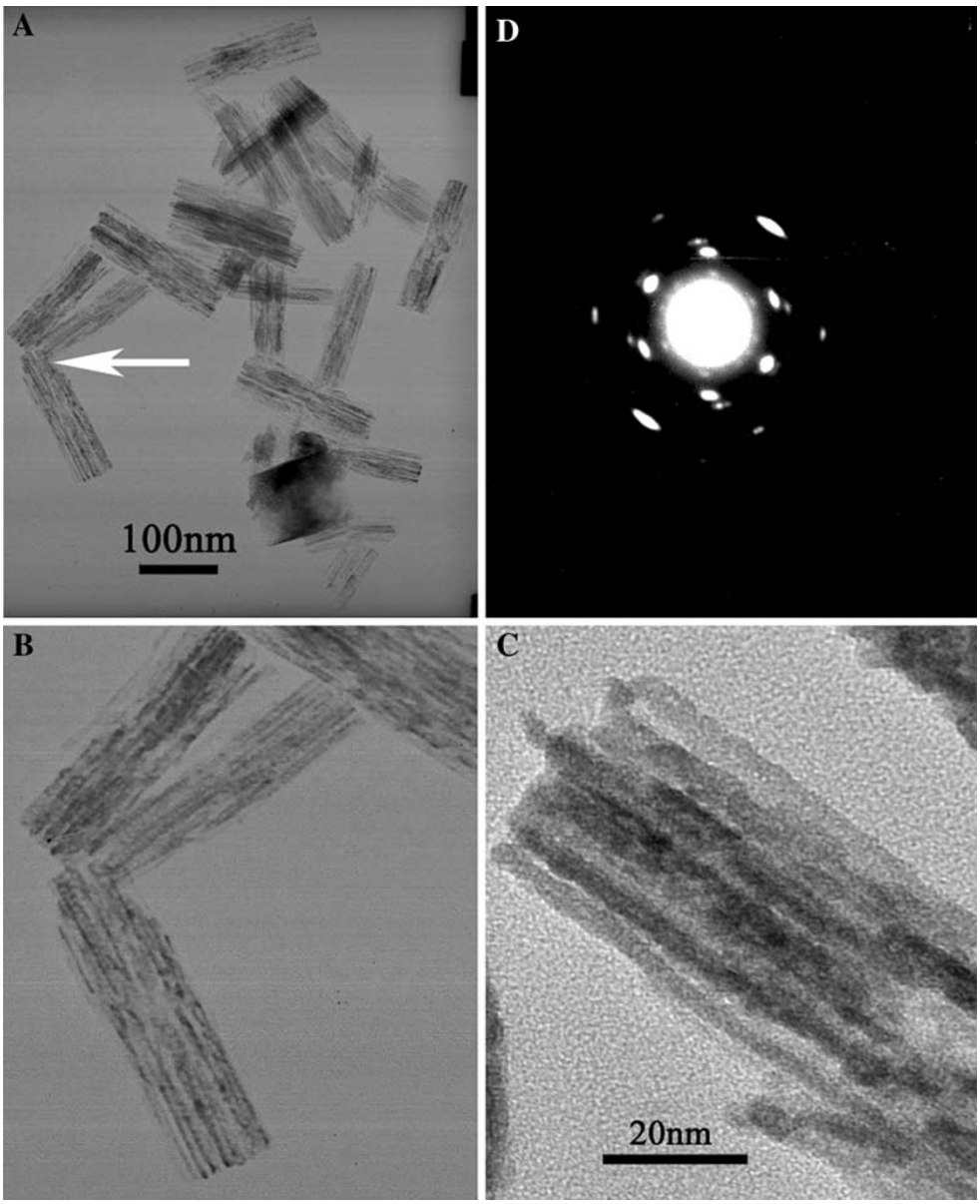

Fig. 3 **a** The typical TEM image of the as-obtained product In_2O_3. **b** The enlarged image of the area marked by the *white arrow* in **a**. **c** TEM image with larger magnification. **d** The selected area electronic diffraction pattern of the resultant product In_2O_3

the TGA/DTA analyses, the existence of CTAB molecules is determined and its content is about 6%. It is well known that the fabrication of the tubular nanomaterials is usually achieved by two strategies: one is the use of hard templates, which involves the removal of the templates, and the other is the use of capping agents/surfactants during nanoparticles growth. Therefore, we speculate that in the present synthetic system, surfactant CTAB, acting as the structure-directing agent, may form 1D micelle structures, further resulting in the formation and self-assembly of the 1D $In(OH)_3$ nanotubes. The assembly mechanism is similar to those nanoparticle micelle structures reported by Fan [11], differing from that reported by Xue [12, 13].

Optical absorption spectrum of the obtained In_2O_3 nanotube bundles was carried out on a HEλIOS*a* spectrometer at room temperature. For comparison, the UV–Vis feature of the commercial In_2O_3 powders was also given. As shown in Fig. 6, the obtained In_2O_3 nanotube bundles, compared with the commercial In_2O_3 powders, take place an evident blueshift of the absorption band edge, which is caused by the increasing energy gap resulted from decreasing the grain size.

In order to further understand the optical nature of In_2O_3 nanotube bundles, the room PL spectrum was measured and the corresponding result was shown in Fig. 7. As can be seen from the Figure, a broad and relatively strong PL

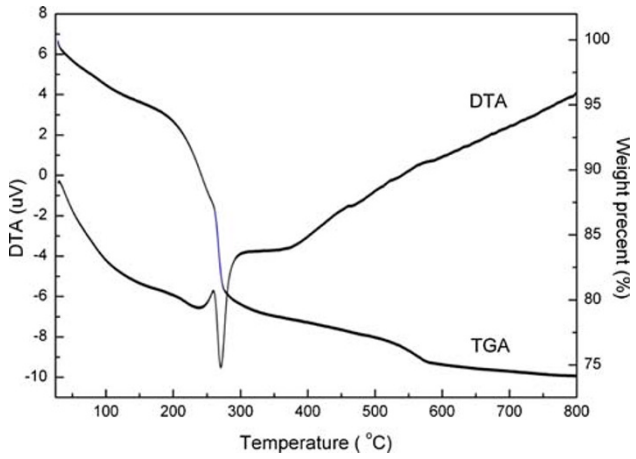

Fig. 4 TGA/DTA curves of the precursor $In(OH)_3$

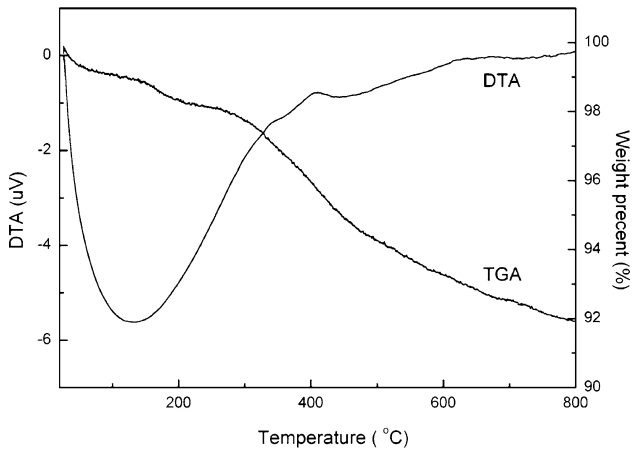

Fig. 5 TGA/DTA curves of the final product In_2O_3

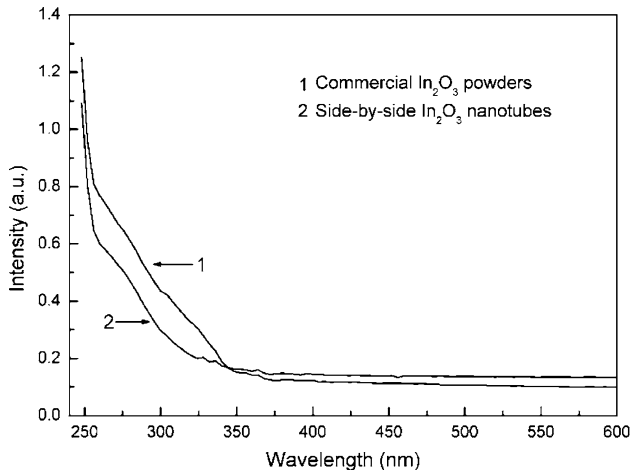

Fig. 6 The UV–Visible absorption spectra of the synthesized side-by-side In_2O_3 nanotubes

emission peak is observed, which is mainly located in the purple–blue region with its maximum intensity centered at 440 nm. This is different from that reported by Li and

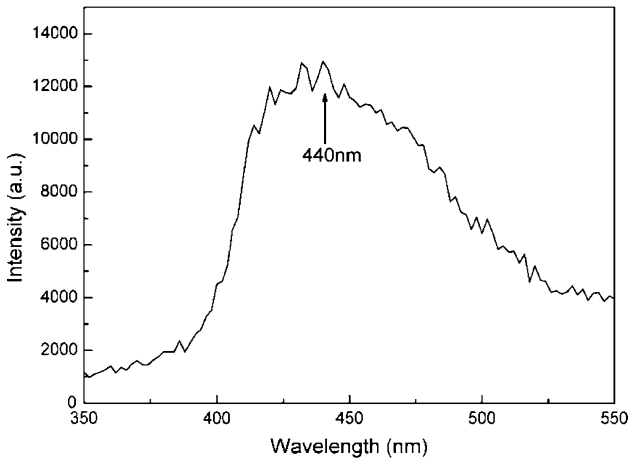

Fig. 7 The room temperature PL spectrum of the obtained side-by-side In_2O_3 nanotubes

coworkers [36]. In Fig. 7, the PL emission of In_2O_3 nanotube bundles was mainly attributed to the effect of the oxygen vacancies. The oxygen vacancies can act as donors and would induce the formation of new energy levels in the band gap. The emission thus can be attributed to the recombination of electrons in singly occupied oxygen vacancies with photoexcited holes.

Conclusion

In conclusion, a simple and mild wet-chemical route we proposed is propitious to the preparation of 1D $In(OH)_3$ nanotube bundles. Furthermore, the morphology of the nanotube bundles was also inherited in the transformation from $In(OH)_3$ to In_2O_3 successfully. Their composition and single-crystalline structures were confirmed using XRD, TEM, and SAED. The optical determinations imply that the UV–Visible and PL behaviors of In_2O_3 nanotube bundles were different from those of the bulk. This means that the as-prepared In_2O_3 nanotube bundles may perform better in optoelectronic devices and nanoscale gas sensors. In addition, on the basis of the present work, we conclude that through the appropriate modification of the synthetic condition, $In(OH)_3$ nanobelts are possibly obtained and further transform into In_2O_3 nanobelts. This work is currently in progress.

Acknowledgments This work is supported by the National Natural Science Foundation of China (Grant No. 50701016).

References

1. C.H. Lu, L.M. Qi, J.H. Yang, D.Y. Zhang, N.Z. Wu, J.M. Ma, J. Phys. Chem. B **108**, 17825 (2004)
2. Y.J. Xiong, Z.Q. Li, R. Zhang, Y. Xie, J. Yang, C.Z. Wu, J. Phys. Chem. B **107**, 3697 (2003)
3. Z.Q. Li, Y.J. Xiong, Y. Xie, Inorg. Chem. **42**, 8105 (2003)
4. Z.Z. Zhang, D. Gekhtman, M.S. Dresselhaus, J.Y. Ying, Chem. Mater. **11**, 1659 (1999)
5. J.W. Wang, Y.D. Li, Adv. Mater. **15**, 445 (2003)
6. M.Y. Yen, C.W. Chiu, C.H. Hsia, F.R. Chen, J.J. Kai, C.Y. Lee, H.T. Chiu, Adv. Mater. **15**, 235 (2003)
7. H. Choi, S.H. Park, J. Am. Chem. Soc. **126**, 6248 (2004)
8. Y.G. Sun, Y.N. Xia, Adv. Mater. **16**, 264 (2004)
9. D.W. Wang, H.J. Dai, Angew. Chem. Int. Ed. **41**, 4783 (2002)
10. C.L. Yan, J. Lin, F. Liu, J.S. Wu, K. Gao, D.F. Xue, Nanoscale Res. Lett. **3**, 473 (2008)
11. H.Y. Fan, Chem. Commun. **12**, 1383 (2008)
12. C.L. Yan, D.F. Xue, Adv. Mater. **20**, 1055 (2008)
13. C.L. Yan, D.F. Xue, Electrochem. Commun. **9**, 1247 (2007)
14. J. Lin, H. Xia, D.F. Xue, L. Lu, J. Am. Chem. Soc. **131**, 12086 (2009)
15. J. Lin, F. Liu, K. Gao, J.S. Wu, D.F. Xue, J. Mater. Chem. **19**, 6073 (2009)
16. J. Lin, D.F. Xue, Adv. Mater. **20**, 2622 (2008)
17. S. Avivi, Y. Mastai, A. Gedanken, Chem. Mater. **12**, 1229 (2000)
18. A. Murli, A. Barve, V.J. Leppert, S.H. Risbud, I.M. Kennedy, H.W.H. Lee, Nano Lett. **1**, 287 (2001)
19. Q. Tang, W.J. Zhou, W. Zhang, S.M. Ou, K. Jiang, W.C. Yu, Y.T. Qian, Cryst. Growth Des. **5**, 147 (2005)
20. A. Gurlo, N. Barsan, U. Weimar, M. Ivanovskaya, A. Taurino, P. Siciliano, Chem. Mater. **15**, 4377 (2003)
21. C. Li, D.H. Zhang, S. Han, X.L. Liu, T. Tang, C.W. Zhou, Adv. Mater. **15**, 143 (2003)
22. O.M. Berengue, A.J.C. Lanfredi, L.P. Pozzi, J.F.Q. Rey, E.R. Leite, A.J. Chiquito, Nanoscale Res. Lett. **4**, 921 (2009)
23. M. Zervos, D. Tsokkou, M. Pervolaraki, A. Othonos, Nanoscale Res. Lett. **4**, 526 (2009)
24. A. Othonos, M. Zervos, D. Tsokkou, Nanoscale Res. Lett. **4**, 491 (2009)
25. C.G. Granqvist, Appl. Phys. A **57**, 19 (1993)
26. K. Sreenivas, T.S. Rao, A. Mansingh, J. Appl. Phys. **57**, 384 (1985)
27. Y. Shigesato, S. Takaki, T. Haranoh, J. Appl. Phys. **71**, 3356 (1992)
28. C.C. Wu, C.I. Wu, J.C. Sturm, A. Kahn, Appl. Phys. Lett. **70**, 1348 (1997)
29. T. Takada, K. Suzukik, M. Nakane, Sens. Actuators B **13**, 404 (1993)
30. I. Hamburg, C.G. Granqvist, J. Appl. Phys. **60**, R123 (1986)
31. J. Zhang, X. Qing, F.H. Jiang, Z.H. Dai, Chem. Phys. Lett. **371**, 311 (2003)
32. J.Y. Lao, J.Y. Huang, D.Z. Wang, Z.F. Ren, Adv. Mater. **16**, 65 (2004)
33. Y.P. Fang, X.G. Wen, S.H. Yang, Angew. Chem. Int. Ed. **45**, 4655 (2006)
34. J. Yang, C.L. Lin, Z.L. Wang, J. Lin, Inorg. Chem. **45**, 8973 (2006)
35. W.H. Ho, S.K. Yen, Thin Solid Films **498**, 80 (2006)
36. Y.B. Li, Y. Bando, D. Golberg, Adv. Mater. **15**, 581 (2003)